PHYSICAL REVIEW B **92**, 100304(R) (2015)

Space-time gradient metasurfaces

Y. Hadad, D. L. Sounas, and A. Alu*

Department of Electrical and Computer Engineering, The University of Texas at Austin, 1616 Guadalupe Street, UTA 7.215, Austin, Texas 78701, USA

(Received 25 February 2015; revised manuscript received 2 September 2015; published 22 September 2015)

Metasurfaces characterized by a transverse gradient of local impedance have recently opened exciting directions for light manipulation at the subwavelength scale. Here we add a temporal gradient to the picture, showing that spatiotemporal variations over a surface may greatly extend the degree of wave manipulation in metasurfaces, and break several of their constraints associated with symmetries. As an example, we synthesize a nonreciprocal classical analog to electromagnetically induced transparency, opening a narrow window of one-way efficient transmission in an otherwise opaque surface. These properties pave the way to magnetic-free, planarized, nonreciprocal ultrathin surfaces for free-space isolation.

DOI: 10.1103/PhysRevB.92.100304 PACS number(s): 78.67.Pt, 42.25.Gy, 42.79.Dj, 42.50.Gy

Snell's law of reflection and refraction describes the fact that at the interface between two homogeneous media the wave momentum is conserved. Transversely inhomogeneous frequency-selective surfaces at radio frequencies and gradient optical metasurfaces have been recently proposed to bypass the conventional form of Snell's law by introducing clever transverse spatial modulations that can add an abrupt additional momentum discontinuity to the incident wave, yielding unusual scattering responses and "generalized refraction laws" over a surface [1–16]. While these concepts have opened a plethora of interesting possibilities for physicists and engineers, allowing manipulation of light over a thin surface, there are fundamental constraints that a gradient metasurface cannot overcome. For instance, a thin electric surface is inherently limited in the amount of energy that it can couple into an anomalously refracted beam due to geometrical symmetries [2], requiring the use of thicker geometries or stacks.

Another fundamental constraint that gradient metasurfaces have to comply with is associated with reciprocity and time-reversal symmetry,

$$R_{ii}(\theta_2,\theta_1) = R_{ii}(\theta_1,\theta_2), \quad T_{ji}(\theta_2,\theta_1) = T_{ij}(\theta_1,\theta_2), \qquad (1)$$

where $R_{ii}(\theta_2,\theta_1)$ [$T_{ji}(\theta_2,\theta_1)$] is the reflection (transmission) coefficient for a plane wave impinging on a surface from the ith region with angle θ_1 to a plane wave that is reflected (transmitted) to the ith (jth) region, with angle θ_2 [Fig. 1(a)]. Equation (1) states that, if we are able to transmit energy through a surface at a particular angle and refract or reflect it towards a specific direction, a plane wave with the same transverse momentum coming back from that direction will couple as well to the original plane wave. These constraints may be overcome only by breaking time-reversal symmetry, which is possible using magneto-optical effects [17], nonlinearities [18], or spatiotemporal modulation [19–25] and moving media [26–28]. Magneto-optical effects require bulky magnets and are difficult to access at optical frequencies, while nonlinearities are power dependent and require electrically large volumes. Furthermore, previously reported solutions for nonreciprocity have been typically limited to waveguide (closed) geometries, and do not allow full transmission, achieving isolation at the price of significant forward insertion loss. In this Rapid Communication, we show that it is possible to overcome the symmetry-related limitations of conventional metasurfaces with spatial gradients by adding transverse *temporal* gradients. For the sake of clarity and mathematical tractability, we restrict ourselves to the simplest gradient impedance surface–a sinusoidally modulated impedance. However, we emphasize that the results developed here are extendable to any type of transverse gradients, as sophisticated as in [1–16].

By combining the concept of temporal and spatial gradients in ultrathin metasurfaces, we create an anomalous nonreciprocal electromagnetically induced transparency (EIT) effect. EIT was introduced in quantum optics as a technique to enhance nonlinear effects, while having strong transmission of the laser beam [29,30]. Its potential applications are vast, as this mechanism allows slow group velocities that can spatially compress the impinging pulse shape and enhance light-matter interactions [31,32]. Classical analogues of the EIT phenomenon, all reciprocal, have been studied in recent years to apply these unusual wave properties to optical devices and metamaterials [33–35]. Here we realize a nonreciprocal EIT-like transmission window through an ultrathin metasurface characterized by transverse spatiotemporal gradients, based on efficient light coupling that overcomes the constraints in Eq. (1). Interestingly, at the proposed EIT peak the transmission amplitude can be made unitary, beyond the previously mentioned symmetry constraints of ultrathin surfaces, and at the same time largely nonreciprocal, yielding, in the absence of loss, an ideal free-space isolator without forward insertion loss.

To demonstrate the proposed concept we consider the transmission and reflection properties of a spatiotemporally modulated metasurface lying on the $x = 0$ plane, described by the time-dependent surface-impedance Lorentzian operator

$$Z_s[i(z,t)] = \{L_0\partial_t i(z,t) + C_0^{-1}[1 - m\cos(\beta z - \Omega t)] \times \int^t i(z,t')dt'\}, \qquad (2)$$

which models a distributed series network of inductors L_0 and spatiotemporally modulated capacitors $C(z,t) = C_0 + \Delta C\cos(\beta z - \Omega t)$, and is applied to the surface current distribution $i(z,t)$. Ω and β are the temporal and spatial

*alu@mail.utexas.edu

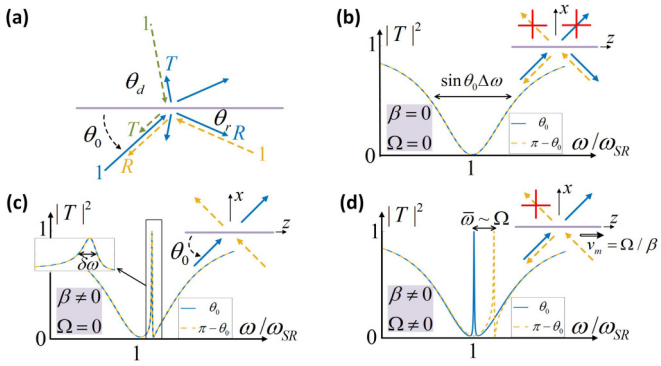

FIG. 1. (Color online) Illustration of the concept. (a) Reciprocity constraints of a reciprocal surface with spatial gradients. The purple horizontal line represents the surface impedance. (b) Typical transmission through the surface impedance in Eq. (2) without modulation. (c) Spatial modulation produces a reciprocal EIT-like transmission. (d) Spatiotemporal modulation provides isolation.

modulation frequencies. Expression (2) holds under the assumption of weak modulation index, i.e., $m \equiv \Delta C/C_0 \ll 1$. For the moment we neglect loss, which may be included by introducing a small series resistance [36]. We neglect spatial dispersion effects, assuming that the surface is composed of deeply subwavelength inclusions.

For the sake of brevity, we consider only transverse-magnetic (TM) excitation; the transverse-electric solution may be found similarly. The incident magnetic field is y polarized with longitudinal wave number $k_z = k\cos\theta, k = \omega/c$, under an $e^{-i\omega t}$ time convention. c is the speed of light. The angle θ is measured from the negative z axis, as shown in Fig. 1. The reflected and transmitted fields do not need to comply with the conventional Snell's law of refraction, due to the transverse gradients, and are generally written as infinite series of Floquet harmonics in both *space* and *time*: $\vec{H}^{t,r} = \hat{y}\sum_{n=-\infty}^{\infty} H_n^{t,r} e^{i(k_{z_n} z \pm k_{x_n} x - \omega_n t)} + \text{c.c.}$ [see Eq. (S2) in [36]]. The superscripts t (r) denote transmitted (reflected) fields and correspond to the upper (lower) signs; $k_{x_n} = \sqrt{k_n^2 - k_{z_n}^2}$ is the transverse wave number and, to satisfy the radiation condition, $\text{Im}\{k_{x_n}\} \geqslant 0$. The radial frequency, wave number, and longitudinal wave number of the nth harmonic are $\omega_n = \omega + n\Omega$, $k_n = \omega_n/c$, and $k_{z_n} = k_z + n\beta$, respectively.

Due to the electric-field continuity across the metasurface, the zeroth-order reflected and transmitted fields, which propagate at angles $\theta_r = \pi - \theta_i$ and $\theta_t = \theta_i$ respectively, are the strongest ones. However, this is not a fundamental constraint and it may be overcome by combining electric and magnetic metasurfaces [5,8], or stacking metasurfaces [2]. The higher-order harmonics have different transverse momentum and frequencies than the incident wave. By enforcing the impedance boundary condition $Z_s\hat{x} \times [\vec{H}|_{x=0^+} - \vec{H}|_{x=0^-}] = \vec{E}_{\tan}|_{x=0}$, we obtain

$$A_n H_n^r - mZ_{c_{n+1}} H_{n+1}^r - mZ_{c_{n-1}} H_{n-1}^r = \delta_n H_0 \eta_0 k_{x_n}/k_n, \quad (3)$$

where $H_n^t = -H_n^r + H_0\delta_n$ and δ_n is the Kronecker delta, $A_n = (2Z_n + \eta_0 k_{xn}/k_n)$, $Z_n = -i\omega_n L_0 + Z_{c_n}$, and $Z_{c_n} = -1/i\omega_n C_0$. Z_n and Z_{c_n} are the metasurface and capacitor impedances associated with the nth harmonic. Equation (3) represents an infinite set of linear equations, which, in the case of weak modulation, may be truncated to the first three harmonics $n = 0, \pm 1$ [36].

In the absence of modulation, $m = 0$, the impedance is zero at the surface resonance $\omega_{\text{SR}} = 1/\sqrt{L_0 C_0}$ and the surface is fully reflective, as shown in Fig. 1(b). When spatial modulation is introduced ($\beta \neq 0$), the surface becomes transparent in a narrow frequency band for a specified incidence direction, exhibiting an EIT-like transmission window, as shown in Fig. 1(c), produced by the coupling of the broad surface resonance and a sharp grating resonance. Yet, in the absence of temporal modulation ($\Omega = 0$), the response remains reciprocal and two full transmission peaks, corresponding to incidence angle θ_0 and its complementary $\pi - \theta_0$, take place at the same frequency ω, namely, $T(\omega,\theta_0) = T(\omega,\pi - \theta_0) = 1$. $T(\omega,\theta)$ corresponds to zeroth-order transmission. The metasurface symmetries require this response, in agreement with Eq. (1) [37]. Once a transverse temporal modulation at frequency Ω is considered, reciprocity breaks, and the two resonance peaks separate by $\bar{\omega} \sim \Omega$, as shown in Fig. 1(d), creating the opportunity for great isolation. Interestingly, as shown below, the bandwidth of the EIT transmission peak $\delta\omega \propto m^2$ decreases with the modulation index m. Counterintuitively, therefore, nonreciprocity is enhanced as m decreases. For a specified, arbitrarily small, Ω, in the absence of losses, it is always possible to find m resulting in large isolation.

To prove these properties, we solve Eq. (3) for the reflection coefficient $R = H_0^r/H_0$ [36],

$$R^{-1} = (k/\eta_0 k_x)[A_0 - m^2 Z_{c0} Z_{c1}/A_1 - m^2 Z_{c0} Z_{c-1}/A_{-1}]. \quad (4)$$

Interestingly, *full transmission* of the zeroth diffraction order and identically *zero coupling* to higher diffraction orders take place if $A_1 = 0$ or $A_{-1} = 0$. These conditions correspond to the resonant excitation of the $1, -1$ diffraction order, and may be regarded as generalized Wood's anomalies for space-time gradient surfaces. The incident wave excites a leaky-wave resonance in the structure, which, by coupling with the spectrum of radiated modes, is able to cancel specular reflections and fully restore the incident power into the fundamental (zeroth-order) transmission angle. Consequently, a narrow transmission window is created within an angle-frequency region for which the unmodulated surface would be opaque. Depending on whether the leaky-wave resonance coincides with the resonance of the nonmodulated surface or not, the transmission window has a symmetrical EIT-like or an asymmetrical Fano-like [38] line shape, as seen in Figs. 1(c) and 1(d). The resonance quality factor, denoted by Q_{FT}, is proportional to the leaky-mode decay rate, and in order to have full-transmission, transverse momentum matching is essential between the incident wave and the leaky mode, i.e., $k\cos\theta_0 = \text{Re}\{k_z^L\}$. k_z^L is the leaky-mode longitudinal wave number. Remarkably, the full transmission property is an exact result of (3), and not an artifact of the weak modulation approximation [36].

Figures 2(a) and 2(b) show the complex dispersion of the transverse wave vector for the zeroth- and first-order harmonics of the TM surface and leaky modes, respectively, supported by a surface with $L_0 = \eta_0 Q/2\omega_{\text{SR}}$ and

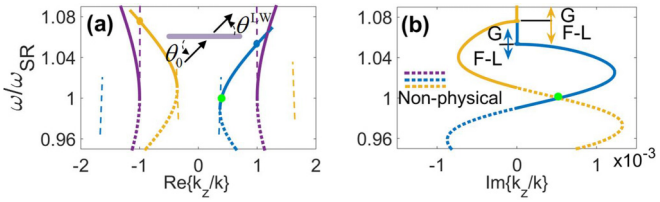

FIG. 2. (Color online) Dispersion of the surface TM modes. (a) Continuous (dotted) lines describe the dispersion of physical (nonphysical) modes. Purple curves correspond to TM modes on the unmodulated surface. Blue and yellow curves correspond to a spatiotemporally modulated surface with $\beta/k = 0.637, \Omega/\omega_{SR} = 0.01$, and $m = 0.01$. Purple, yellow, and blue dashed lines represent the light cone for the $n = 0$, $n = 1$ and $n = -1$ harmonics, respectively. (b) Imaginary part of the mode wave number. The light-green circle indicates the operation point for the results in Fig. 3. The inset in (a) illustrates the enforced excitation of a leaky mode by a plane wave.

$C_0 = 2/\eta_0 Q\omega_{SR}$, where $Q = 10$ is the surface quality factor, $m = 0.01$, $\beta/k = 0.637$, and $\Omega/\omega_{SR} = 0.01$, and η_0 is the free-space impedance [39]. The dispersion was derived by calculating the complex k_z roots of Eq. (3) with $H_0 = 0$. The continuous (dotted) lines refer to the dispersion of physical (nonphysical) modes, which can be significantly (weakly) excited by physical sources [36,38,40,41]. Physical modes include guided (G) and leaky-forward (L-F) with $v_g v_p > 0$.

Without modulation, the surface dispersion is real and symmetric, and limited to the range $\omega > \omega_{SR}$, since TM modes are supported by inductive surfaces. These modes are guided, and cannot couple to free-space radiation. Spatial modulation allows coupling surface modes to radiation through higher-order harmonics, generating the EIT transparency window, but still preserving the dispersion symmetry. In this scenario, the dispersion diagram consists of an infinite set of propagation branches in both directions, shifted by β with respect to each other [36].

The dispersion symmetry is lifted, and reciprocity is violated, when a temporal gradient is added, which shifts vertically the nth Floquet harmonic by $n\Omega$. Then, the cutoff frequency of the leaky harmonics, which are responsible for coupling to the radiation continuum, is different by 2Ω for opposite propagation directions, as seen in Fig. 2 (blue and yellow lines). Consequently, with proper design it is possible to excite the supported leaky mode and achieve a transparency window from one direction, but not from its complementary direction.

For example, at frequency $\omega = \omega_{SR}$ one physical solution exists, $k_z/k = 0.3949 + 5.5 \times 10^{-4} i$ (light green point in Fig. 2), corresponding to a highly directive leaky mode, radiating towards $\theta^{LW} = \cos^{-1}(0.3949) = 66.74^\circ$. Therefore, an incident wave at $\theta_0 = \theta^{LW}$ $(\pi - \theta_0)$ would couple (poorly couple) with this mode [see the inset of Fig. 2(a)], and Eq. (4) yields full transmission (high isolation). This is direct evidence of strong nonreciprocity and isolation [37].

The incidence angles for which full-transmission occurs can be calculated in closed-form using $A_1 = 0$ or $A_{-1} = 0$. In particular, assuming that $\omega \approx \omega_{SR}$ [36], we obtain four solutions. Two are

$$\cos\theta_0 \simeq \pm\sqrt{1 + [2(d\omega + \Omega)/\Delta\omega]^2} - \beta/k \qquad (5)$$

and the other two are obtained by replacing $-\Omega \mapsto \Omega$ and $-\beta \mapsto \beta$ in (5). Here, $\Delta\omega = \omega_{SR}/Q$ is the bandwidth of the unmodulated surface for normal incidence, and $d\omega = \omega - \omega_{SR}$ is the frequency detuning from the resonance of the unmodulated surface. Equation (5) is valid if and only if: (a) either the $+1$ or -1 diffraction order is evanescent within the visible angular spectrum $|k_z| < \omega/c$, i.e., $(\omega \pm \Omega)/c < |k_z \pm \beta|$, and at the same time (b) the surface impedance is inductive for that harmonic, i.e., $\omega > \omega_{SR} \mp \Omega$. The latter is equivalent to working above the cutoff frequencies of the physical leaky modes. Equation (5) clearly shows that spatial modulation is enough to achieve angularly selective transmission, but cannot break time-reversal symmetry and the constraint in (1). The transparency window will necessarily occur at both θ_0 and $\pi - \theta_0$. Angularly selective *nonreciprocal* transmission will be obtained only by realizing a transverse spatiotemporal gradient on the surface. For the set of parameters in Fig. 2, Eq. (5) is satisfied only for $\theta_0 = 66.74^\circ$, confirming our predictions based on the dispersion diagram in Fig. 2 (see also [36] Sec. 2.1). Interestingly, the full-transmission angle is independent of the modulation index m, which, as shown below, affects only the bandwidth of the transparency window.

Figure 3 shows the power transmission $|T|^2$ towards the zeroth diffraction order versus frequency for the incidence directions $\theta_0 = 66.74^\circ$ and $180^\circ - \theta_0 = 113.26^\circ$, and the corresponding magnetic field profiles at frequency ω_{SR}. The transmission was calculated analytically through Eq. (4) and numerically using finite-difference time-domain (FDTD) simulations. The field profiles were derived through FDTD simulations. We used the same parameters as in Fig. 2, except for the modulation index which is $m = 0.05$. Such an increase

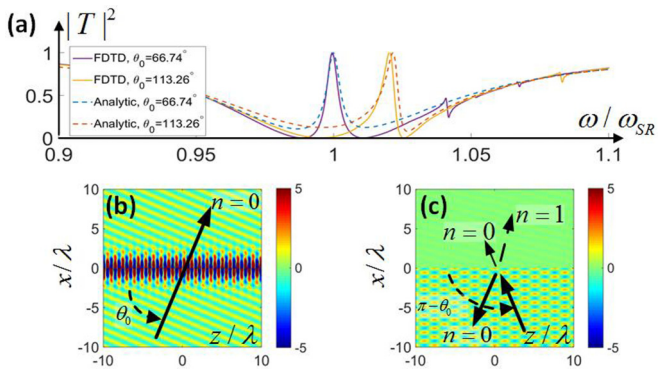

FIG. 3. (Color online) Nonreciprocal surface response. (a) Transmission vs frequency for complementary incident waves at $\theta_0 = 66.74^\circ$ and $180^\circ - \theta_0 = 113.26^\circ$. The response was calculated by FDTD simulation and analytically. Parameters: $\Omega/\omega_{SR} = 0.01, m = 0.05, \beta/k = 0.637$. (b) Magnetic field profile for $\omega = \omega_{SR}$ and $\theta_0 = 66.74^\circ$, when full transmission takes place. The reactive energy near the surface is large due to the enforced excitation of a weakly radiating leaky mode. No other propagating diffraction order is excited. (c) As (b), but for excitation from $180^\circ - \theta_0$. No leaky mode is excited; the surface is practically opaque. The $n = 1$ harmonic is weakly excited at a different frequency than the incident wave.

in m reduces only the EIT-like resonance Q factor, thereby reducing the FDTD simulation time.

For incidence at $\theta_0 = 66.74°$, the transmission peaks at $\omega = \omega_{SR}$, consistent with the existence of a leaky mode at the light-green point in Fig. 2. However, for incidence at $180° - \theta_0 = 113.26°$ the transparency window is blueshifted $\omega = 1.02\omega_{SR}$, due to the blueshift of the leaky mode propagating along the $-z$ direction in Fig. 2. The field profiles in Figs. 3(b) and 3(c) verify that power is almost completely transmitted (reflected) for incidence from $\theta_0 = 66.74°$ ($180° - \theta_0 = 113.26°$). The additional higher-order resonances in the FDTD simulation are the result of high-order modulation harmonics, due to the fact that the impedance operator involves the *inverse* of the harmonically-modulated capacitance. Although for $m \ll 1$ the higher-order harmonics are very small and can be neglected in the analytical treatment, they yet have a minor effect in the FDTD simulations.

The strong reactive fields in Fig. 3(b) close to the surface reveal the excitation of a strong resonance, which corresponds to the fundamental Floquet harmonic of the leaky mode in Fig. 2 [42]. Its amplitude can be calculated as $H_1^r = -(\eta_0/Z_{c_1})(k_x/k)H_0/m$, showing that, for $m \ll 1$, it can become much stronger than the incident-field amplitude H_0. However, in the case $180° - \theta_0 = 113.26°$ the reactive fields are very weak, since the coupling between the incident wave and the leaky mode is negligible. In such cases, the impinging energy experiences specular reflection, except for a weak $n = 1$ diffraction order at frequency $\omega = \omega_{SR} + \Omega$ and direction $\theta_1 = \cos^{-1}(k_z^1/k_1) = 76.1°$ with respect to $+\hat{z}$.

The anomalous EIT-like dispersion is a consequence of the interplay between wide resonance of the uniform metasurface and the much narrower resonance associated with the leaky mode produced by the modulation. For a specified θ_0, the EIT-resonance bandwidth and Q factor are approximately

$$\delta\omega = m^2 Q\omega_{SR}/4\sin\theta_0 \rightarrow Q_{FT} = 4\sin\theta_0/m^2 Q, \quad (6)$$

predicting a vanishing bandwidth for infinitely small modulation index. For weak modulation, the lifetime of the surface leaky mode increases and becomes infinite as $m \rightarrow 0$ (bound mode), when no coupling to free space exists, opening the possibility of inducing a nonreciprocal embedded scattering eigenstate on the surface [43,44]. Finite Ohmic loss in practice yields a lower bound on $\delta\omega$, derived as $\min\delta\omega = (\sqrt{2} - 1)\Delta\omega R_O/\eta_0$, where R_O is the distributed surface resistance [36]. For moderate losses the results presented here still hold. The high-Q leaky resonance allows drastic relaxation of the requirements regarding the temporal modulation frequency required to achieve significant isolation. The frequency separation of full-transmission peaks for opposite propagation directions is $\bar{\omega} \approx \Omega + \Delta\omega\sqrt{\Omega/\omega_{SR}}$ [36]. For isolation between θ_0 and $\pi - \theta_0$ we require $\bar{\omega} > \delta\omega$. Therefore, unexpectedly, for a given Ω, a weaker m leads to higher isolation, within the low-loss approximation. Equation (6) also suggests that a lower Q factor for the surface provides a larger resonance Q_{FT}. This is because a lower surface Q implies less sensitivity to the modulation, ensuring less energy leakage for given m. As shown in [36], the angular bandwidth also decreases as m increases, following a similar square power law.

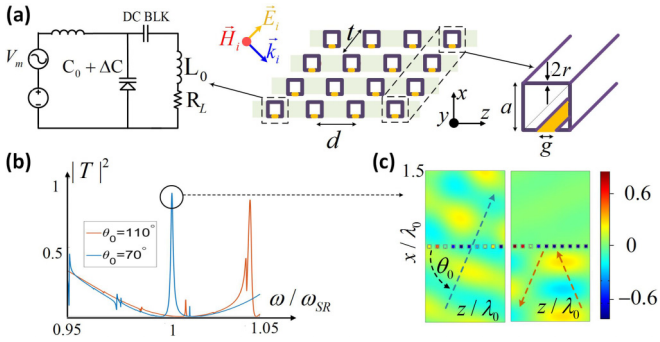

FIG. 4. (Color online) Implementation using an array of split-ring resonators. (a) Metasurface geometry. Left inset: Lumped circuit model for the loaded loop and biasing network. L_0 and R_L are the equivalent inductance and radiation/Ohmic resistance of a single loop. Right inset: Zoom on a single loop as implemented in the finite-element simulation. The gap is filled with a time-varying dielectric (yellow). The side length, gap, and metal thickness of the SRRs were selected as $a = \lambda_0/15$, $g = 0.0046\lambda_0$, and $r = 0.01\lambda_0$, respectively, with λ_0 the resonance wavelength. The modulation periodicity is $D = 2\pi/\beta$, and the lattice periodicity is $d = D/N$, with $N = 10$. (b) Transmission at two complementary angles. (c) Magnetic field at $\omega/\omega_{SR} \approx 1$. Almost full transmission (high isolation) is obtained at $\theta_0 = 70°$ ($\theta_0 = 110°$).

A possible implementation of the surface impedance operator in Eq. (2) involves a two-dimensional (2D) array of split-ring resonators (SRRs) loaded with variable capacitors, as in Fig. 4(a). This realistic structure was analyzed via full-wave finite-element simulations, with variable capacitors implemented by filling the gaps of the nth row of SRRs with time-modulated dielectric material, $\varepsilon_r = \varepsilon_r^0[1 + m\cos(\Omega t - \beta nd)]$, where d is the SRR periodicity. The modulation parameters are $\beta/k = 0.793$, $m = 0.1$, and $\Omega = 0.02\omega_{SR}$. In order to relax the computational requirements of a full 3D simulation, we assumed a distance between SRRs along the y direction $t < d \ll \lambda_0$, and replaced 1D arrays with an equivalent 2D SRR, as in Fig. 4(a). The particles are lossy, made of copper. The power transmission is given in Fig. 4(b); its peaks are about 85%–90% due to Ohmic loss. The nonreciprocal EIT-like response of the structure is evident. From Fig. 4(b) the surface bandwidth is estimated as $\Delta\omega \approx 0.2\omega_{SR}$, implying $Q \approx 5$. From Eq. (S33) [36], $\bar{\omega} \approx 0.048$, and from Eq. (5) $\theta_0 \approx 77.76°$, in good agreement with the simulation results. Moreover, from Fig. 4(b) $\delta\omega \approx 0.002\omega_{SR}$, which, when substituted into Eq. (6), yields an effective modulation index $m_{\text{eff}} \approx 0.038$. Note that $m_{\text{eff}} < m$ due to the discrete nature of the surface and additional parasitic capacitances, making $\delta\omega$ smaller than what would ideally be expected. The additional transmission resonances are due to higher-order modulation harmonics. The left panel of Fig. 4(c) shows the magnetic field distribution at the maximum-transmission frequency for an incidence angle of 70°, showing large transmission and almost zero reflection. The right panel corresponds to the complementary incident angle 110°, for which transmission is very small. The proposed rf structure in Fig. 4(a) may be practically realized using split-ring resonators loaded by varactors, which work well up to the gigahertz range and can provide a wide range of modulation indices. In

acoustics, modulation can be achieved through piezoelectric components as in [45], and in IR or optics, the modulation can be imparted via carrier injection, acousto-optical effects, or parametric modulation of nonlinear media through strong laser pulses. We emphasize however that, as opposed to the rf and acoustic implementations, IR and optical implementations may be challenging, considering that the corresponding designs need to balance the requirement of sufficiently high quality factor and the ability to modulate the optical response.

To conclude, in this Rapid Communication we extended the concept of graded metasurfaces by adding transverse temporal modulation to the electronic properties of surface impedance. We showed that spatiotemporal modulation can overcome geometrical symmetry constraints of ultrathin surfaces, yielding nonreciprocal, angularly selective, full transmission through an ultrathin impedance surface. In our proof of concept scenario, we focused on relatively simple periodic space-time gradients; however, this concept can be readily extended and applied to more sophisticated surfaces with impedance gradients that enable further control of light as in [1–16]. The proposed concept of space-time gratings can also be used to enhance control over near fields and to create nonreciprocal radiation [46,47], opening additional venues for efficient source-field manipulation.

This work was supported by the Air Force Office of Scientific Research with Grant No. FA9550-14-1-0105 and the Defense Threat Reduction Agency with Grant No. HDTRA1-12-1-0022, and by the Office of Naval Research.

[1] N. Yu, P. Genevet, M. A. Kats, F. Aieta, J.-P. Tetienne, F. Capasso, and Z. Gaburro, Light propagation with phase discontinuities: Generalized laws of reflection and refraction, Science **334**, 333 (2011).

[2] F. Monticone, N. M. Estakhri, and A. Alu, Full Control of Nanoscale Optical Transmission with a Composite Metascreen, Phys. Rev. Lett. **110**, 203903 (2013).

[3] Y. Li, X. Jiang, R.-Q. Li, B. Liang, X.-Y. Zou, L.-L. Yin, and J.-C. Cheng, Experimental Realization of Full Control of Reflected Wave with Subwavelength Acoustic Metasurfaces, Phys. Rev. Appl. **2**, 064002 (2014).

[4] K. Sarabandi and N. Behdad, A frequency selective surface with miniaturized elements, IEEE Trans. Ant. Prop. **55**, 1239 (2007).

[5] C. Pfeiffer and A. Grbic, Millimeter-wave transmitarrays for wavefront and polarization control, IEEE Trans. Microwave Theory and Techniques **61**, 4407 (2013).

[6] M. Selvanayagam and G. V. Eleftheriades, Circuit modelling of Huygens surfaces, IEEE Ant. Wireless Prop. Lett. **12**, 1642 (2013).

[7] M. Selvanayagam and G. V. Eleftheriades, Discontinuous electromagnetic fields using orthogonal electric and magnetic currents for wavefront manipulation, Opt. Express **21**, 14409 (2013).

[8] C. Pfeiffer and A. Grbic, Metamaterial Huygens' Surfaces: Tayloring Wave Fronts with Reflectionless Sheets, Phys. Rev. Lett. **110**, 197401 (2013).

[9] D. Sievenpiper, J. Schaffiner, R. Loo, G. Tangonan, S. Ontiveros, and R. Harold, A tunable impedance surface performing as a reconfigurable beam steering reflector, IEEE Trans. Ant. Prop **50**, 384 (2002).

[10] E. Hasman, V. Kleoner, G. Biener, and A. Niv, Polarization dependent focusing lens by use of quantized Pancharatnam-Berry phase diffractive optics, Appl. Phys. Lett. **82**, 328 (2003).

[11] Dianmin Lin, Pengyu Fan, Erez Hasman, and Mark L. Brongersma, Dielectric gradient metasurface optical elements, Science **345**, 298 (2014).

[12] O. Avayu, O. Eisenbach, R. Ditcovski, and T. Ellenbogen, Optical metasurfaces for polarization controlled beam shaping, Opt. Lett. **39**, 3892 (2014).

[13] C. L. Holloway, M. A. Mohamed, E. F. Kuester, and A. Dienstfrey, Reflection and transmission properties of metafilm: With an application to controllable surface composed of resonant particles, IEEE Trans. Electromagn. Compat. **47**, 853 (2005).

[14] E. F. Kuester, M. A. Mohamed, M. Piket-May and C. L. Holloway, Averaged transition conditions for electromagnetic fields at a metafilm, IEEE Trans. Ant. Prop. **51**, 2641 (2003).

[15] N. Meinzer, W. L. Barnes, and I. R. Hooper, Plasmonic meta-atoms and metasurfaces, Nat. Photonics, **8**, 889 (2014).

[16] V. S. Asadchy, Y. Ra'di, J. Vehmas, and S. A. Tretyakov, Functional Metamirrors Using Bianisotropic Elements, Phys. Rev. Lett. **114**, 095503 (2015).

[17] Y. Mazor and B. Z. Steinberg, Metaweaves: Sector-Way Nonreciprocal Metasurfaces, Phys. Rev. Lett. **112**, 153901 (2014).

[18] A. M. Mahmoud, A. R. Davoyan, and N. Engheta, All-passive nonreciprocal metasurface, arXiv:1407.1812.

[19] Z. Yu and S. Fan, Complete optical isolation created by indirect interband phtonic transitions, Nat. Photonics **3**, 91 (2009).

[20] H. Lira, Z. Yu, S. Fan, and M. Lipson, Electrically Driven Non-Reciprocity Induced by Interband Photonic Transition on a Silicon Chip, Phys. Rev. Lett. **109**, 033901 (2012).

[21] K. Fang and S. Fan, Control the Flow of Light Using Inhomogenous Effective Gauge Field that Emerges from Dynamic Modulation, Phys. Rev. Lett., **111**, 203901 (2013).

[22] Q. Lin and S. Fan, Light guiding by effective gauge field for photons, Phys. Rev. X **4**, 031031 (2014).

[23] D. L. Sounas, C. Caloz, and A. Alu, Giant non-reciprocity at the subwavelength scale using angular momentum-biased metamaterials, Nat. Commun. **4**, 2407 (2013).

[24] D. L. Sounas and A. Alu, Angular momentum biased nanorings to realize magnetic free integrated optical isolation, ACS Photonics **1**, 198 (2014).

[25] N. A. Estep, D. L. Sounas, J. Soric, and A. Alù, Magnetic-free non-reciprocity based on parametrically modulated coupled-resonator loops, Nat. Phys. **10**, 923 (2014).

[26] D. W. Wang, H. T. Zhou, M. J. Guo, J. X. Zhang, J. Evers, and S. Y. Zhu, Optical Diode Made from a Moving Photonic Crystal, Phys. Rev. Lett. **110**, 093901 (2013).

[27] R. Fleury, D. L. Sounas, C. F. Sieck, M. R. Haberman, and A. Alu, Sound isolation and giant linear nonreciprocity in a compact acoustic circulator, Science **343**, 516 (2014).

[28] A. Bahabad, Diffraction from moving grating, Opt. Quantum Electron. **46**, 1065 (2014).

[29] S. E. Harris, J. E. Field, and A. Imamoğlu, Nonlinear Optical Processes Using Electromagnetically Induced Transparency, Phys. Rev. Lett. **64**, 1107 (1990).

[30] K.-J. Boller, A. Imamoğlu, and S. E. Harris, Observation of Electromagnetically Induced Transparency, Phys. Rev. Lett. **66**, 2593 (1991).

[31] C. Liu, Z. Dutton, C. H. Behroozi, and L. V. Hau, Observation of coherent optical information storage in an atomic medium using halted light pulses, Nature (London) **409**, 490 (2001).

[32] D. Budker, D. F. Kimball, S. M. Rochester, and V. V. Yashchuk, Nonlinear Magneto-Optics and Reduced Group Velocity of Light in Atomic Vapor with Slow Ground State Relaxation, Phys. Rev. Lett. **83**, 1767 (1999).

[33] M. F. Yanik, W. Suh, Z. Wang, and S. Fan, Stopping Light in a Waveguide with an All-Optical Analog of Electromagnetically Induced Transparency, Phys. Rev. Lett. **93**, 233903 (2004).

[34] Q. Xu, S. Sandhu, M. L. Povinelli, J. Shakya, S. Fan, and M. Lipson, Experimental Realization of an On-Chip all Optical Analogue to Electromagnetically Induced Transparency, Phys. Rev. Lett. **96**, 123901 (2006).

[35] N. Papasimakis, V. A. Fedotov, N. I. Zheludev, and S. L. Prosvirnin, Metamaterial Analog of Electromagnetic Induced Transparency, Phys. Rev. Lett. **101**, 253903 (2008).

[36] See Supplemental Material at http://link.aps.org/supplemental/10.1103/PhysRevB.92.100304 for detailed derivations of some of the equations in the paper.

[37] Full transmission at θ_0 requires zero specular reflection towards $\pi - \theta_0$. The first of Eq. (1) therefore requires that a reciprocal surface does not reflect also at the complementary angle. Moreover, for a surface symmetric with respect to the normal direction, $T_{ji}(\theta_2,\theta_1) = T_{ij}(\theta_2,\theta_1)$ and the second of Eq. (1) becomes $T_{ji}(\theta_2,\theta_1) = T_{ji}(\theta_1,\theta_2)$. For $\theta_2 = \pi - \theta_1$, it becomes $T_{ji}(\pi - \theta_1,\theta_1) = T_{ji}(\theta_1,\pi - \theta_1)$. $T_{ji}(\pi - \theta,\theta)$ is the transmission coefficient of the zeroth-order spatial harmonic. Therefore, a symmetric reciprocal surface requires the same zeroth-order transmission for incidence from complementary angles.

[38] A. E. Miroshnichenko, S. Flach, and Y. S. Kivshar, Fano-resonances in nanoscale structures, Rev. Mod. Phys. **82**, 2257 (2010).

[39] The surface Q factor is defined assuming that the dominant loss mechanism is radiation towards normal incidence, $Q = \omega_{SR} L_0/(\eta_0/2)$. The definition may be easily modified to take Ohmic loss into account.

[40] A. Hessel and A. A. Oliner, A new theory of Wood's anomalies on optical grating, Appl. Opt. **4**, 1275 (1965).

[41] F. Capolino, *Theory and Phenomena of Metamaterials* (CRC Press, Taylor & Francis group, Boca-Raton, FL, 2009).

[42] The fundamental Floquet harmonic of the leaky mode corresponds to the $+1$ or -1 Floquet harmonic in the case of plane-wave excitation.

[43] C.W. Hsu, B. Zhen, J. Lee, S.-L. Chua, S. G. Johnson, J. D. Joannopoulos, and M. Soljačić, Observation of trapped light within the radiation continuum, Nature (London) **499**, 188 (2013).

[44] F. Monticone and A. Alù, Embedded Photonic Eigenvalues in 3D Nanostructures, Phys. Rev. Lett. **112**, 213903 (2014).

[45] R. Fleury, D. L. Sounas, and A. Alù, Subwavelength ultrasonic circulator based on spatiotemporal modulation, Phys. Rev. B **91**, 174306 (2015).

[46] Y. Hadad and B. Z. Steinberg, One-way optical waveguides for matched non-reciprocal nanoantennas with dynamic beam scaning functionality, Opt. Express **21**, S1A77 (2012).

[47] Y. Hadad, Y. Mazor, and Ben Z. Steinberg, Green's function theory for one-way particle chains, Phys. Rev. B **87**, 035130 (2013).